AIAA JOURNAL
Vol. 45, No. 2, February 2007

Measurement of Nonuniform Temperature Distributions Using Line-of-Sight Absorption Spectroscopy

Xiang Liu,* Jay B. Jeffries,† and Ronald K. Hanson‡
Stanford University, Stanford, California 94305-3032

DOI: 10.2514/1.26708

A laboratory demonstration is reported for two measurement strategies to determine nonuniform temperature distributions in combustion gases using line-of-sight absorption spectroscopy. These strategies rely on measurements of multiple absorption transitions of a single species, each with unique temperature dependence. The first strategy, called profile fitting, mathematically fits the observed absorption measurements constrained with a postulated temperature distribution. The second strategy, called temperature binning, determines the temperature probability density function along the line of sight using prescribed temperature bins. The wavelength-multiplexed sensor concepts and the mathematical representations are first explored in detail. The measurements of a "two-zone" temperature/mole-fraction (T/X_{H2O}) distribution with a wavelength-multiplexed scheme for near-infrared transitions of water vapor are then presented to illustrate the fundamental concepts and investigate the sensor performance. The measured two-zone T/X_{H2O} distribution is composed of a 25.4 cm hot-flame zone ($T \approx 1500$ K, $X_{H2O} \approx 10\%$) and a cold-room-air zone ($T \approx 300$ K, $X_{H2O} \approx 2\%$) of about the same length. The experimental results demonstrate that a nonuniform temperature distribution can be characterized with either strategy. The measurement accuracy will increase with the number of transitions, and also with the use of optimally chosen transitions. The experimental results also confirm that use of known physical constraints to reduce the number of degrees of freedom improves the interpretation of the measurement results and thus the sensor performance.

Nomenclature

A	=	integrated absorbance, cm^{-1}
c	=	speed of light, cm/s
dx	=	differential path length, cm
E''	=	lower-state energy of a transition, cm^{-1}
f_j	=	fraction of path length for each bin
h	=	Planck's constant, J · s
I_t	=	transmitted laser intensity, W/m^2
I_ν	=	laser intensity at frequency ν, W/m^2
I_0	=	incident laser intensity, W/m^2
k	=	Boltzmann's constant, J/K
L	=	total path length, cm
L_b	=	boundary layer thickness, cm
$L_{T\text{char}}$	=	characteristic length associated with nonuniform temperature distribution, cm
$L_{X\text{char}}$	=	characteristic length associated with nonuniform mole-fraction distribution, cm
m	=	number of absorption transitions
n	=	number of temperature bins
P	=	total pressure, atm
$Q(T)$	=	partition function of the absorbing molecule, J/K
R	=	ratio of the integrated absorbances
S_i	=	line strength of transition i, cm^{-2} atm^{-1}
T	=	temperature, K
T_b	=	boundary-layer temperature, K
T_c	=	core flow temperature, K
T_{char}	=	characteristic temperature, K
T_w	=	wall temperature, K
X_{abs}	=	mole fraction of the absorbing species
$X_{\text{abs}}L$	=	column density of the absorbing species
X_{char}	=	characteristic mole fraction
x	=	position along the laser line-of-sight measurement path
α	=	spectral absorbance
ν	=	laser frequency, cm^{-1}
ϕ_ν	=	line-shape function at frequency ν

Presented as Paper 834 at the 44th Aerospace Sciences Meeting, Reno, NV, 1 January 2006; received 21 July 2006; accepted for publication 25 October 2006.

*Research Assistant, High Temperature Gasdynamics Laboratory, Department of Mechanical Engineering. Student Member AIAA.

†Senior Research Engineer, High Temperature Gasdynamics Laboratory, Department of Mechanical Engineering. Associate Fellow AIAA.

‡Professor, High Temperature Gasdynamics Laboratory, Department of Mechanical Engineering. Fellow AIAA.

I. Introduction

LASER absorption spectroscopy has become a successful sensor strategy for fast, nonintrusive, sensitive, and reliable in situ measurements of multiple flowfield parameters such as temperature, pressure, velocity, and species concentration in a variety of practical combustion and propulsion flows [1–6]. However, this line-of-sight (LOS) sensing technique has traditionally been limited to flowfields with nearly uniform properties. In practical flowfields, significant temperature and species concentration gradients may exist along the measurement path for optical diagnostics due to flow mixing, chemical reaction, phase change, heat transfer with the side walls, and other effects. Tomographic reconstruction of laser absorption along multiple LOSs has been demonstrated in laboratory experiments to resolve these nonuniformities [7–10], but practical systems seldom have sufficient optical access and the sensor redundancy necessary for quantitative application of tomographic techniques.

Extension of LOS absorption measurements to nonuniform flowfields has been previously explored, including work to correct for boundary-layer effects [11–13], to reduce sensitivities to flow nonuniformities [12,14], and to correlate pattern factors with the path-averaged temperatures inferred from different line pairs [15,16]. Current efforts build on earlier work of our research group to extract the temperature distribution information from simultaneous measurements of multiple absorption transitions [17]. Here we systematically investigate two strategies for nonuniform temperature distribution measurements using LOS absorption spectroscopy. The first strategy, called profile fitting, solves the characteristic properties of a temperature distribution profile postulated using physical constraints. The second strategy, called temperature binning, determines the temperature probability density function (PDF) along

the LOS using prescribed temperature bins. This paper reports an initial laboratory demonstration of the two strategies. The design rules for the selection of optimal absorption transitions, simulation-based evaluation of the performance as a function of number of transitions, and more extensive validation experiments of this concept are described separately [18]. Here the sensor concepts and the representative mathematical evaluations are discussed. An example experiment using a fiber-coupled multiplexer to combine five laser beams onto a single beam path and fiber-coupled demultiplexer to disperse the collected transmitted light onto five separate detectors illustrates the use of seven absorption transitions to investigate a "two-zone" temperature/mole-fraction distribution. This measurement demonstrates the sensor concepts and is used for preliminary investigations of the sensor performance.

II. Theoretical Principles

The fundamental principles of laser absorption spectroscopy and their application to temperature measurement in uniform flowfields have been discussed in detail previously [1,19]. When collimated light at frequency ν enters a gas sample of differential length dx, the fraction of light that is absorbed can be predicted as follows by the Einstein theory of radiation:

$$\frac{-\mathrm{d}I_\nu}{I_\nu} = PX_{\mathrm{abs}}(x)S_i[T(x)]\phi_\nu\,\mathrm{d}x \tag{1}$$

The line strength S is dependent on the temperature via the lower-state energy E'' of this transition:

$$S(T) = S(T_0)\frac{Q(T_0)}{Q(T)}\left(\frac{T_0}{T}\right)\exp\left[-\frac{hcE''}{k}\left(\frac{1}{T}-\frac{1}{T_0}\right)\right] \times\left[1-\exp\left(\frac{-hc\nu_0}{kT}\right)\right]\left[1-\exp\left(\frac{-hc\nu_0}{kT_0}\right)\right]^{-1} \tag{2}$$

The partition function $Q(T)$ is evaluated using the expressions in [20]. For a total path length of L, the fractional transmission can be inferred from Eq. (1) as

$$\left(\frac{I_t}{I_0}\right)_\nu = \exp\left(-P\int_0^L X_{\mathrm{abs}}(x)S_i[T(x)]\phi_\nu\,\mathrm{d}x\right) \tag{3}$$

The absorbance α is defined as

$$\alpha_\nu \equiv -\ell_n\left(\frac{I_t}{I_0}\right)_\nu = P\int_0^L X_{\mathrm{abs}}(x)S_i[T(x)]\phi_\nu\,\mathrm{d}x \tag{4}$$

Because the line-shape function ϕ_ν is normalized such that $\int_{-\infty}^{\infty}\phi_\nu\,\mathrm{d}\nu \equiv 1$, the integrated absorbance A of transition i can be inferred from Eq. (4) as

$$A_i = \int_{-\infty}^{\infty}\alpha_\nu\,\mathrm{d}\nu = P\int_0^L X_{\mathrm{abs}}(x)S_i[T(x)]\,\mathrm{d}x \tag{5}$$

When the gas medium is uniform, Eq. (3) reduces to the Beer–Lambert's law, which is the most commonly used equation for absorption spectroscopy:

$$\left(\frac{I_t}{I_0}\right)_\nu = \exp[-PX_{\mathrm{abs}}S_i(T)\phi_\nu L] \tag{6}$$

The integrated absorbance is thus simplified to

$$A_i = PX_{\mathrm{abs}}S_i(T)L \tag{7}$$

The uniform gas temperature T can be determined from the ratio of the integrated absorbances of two transitions with different temperature dependence [19]

$$R = \frac{A_1}{A_2} = \frac{S_1(T)}{S_2(T)} \tag{8}$$

As a natural extension, the information on a nonuniform temperature distribution along the LOS can be extracted from the absorption measurements of multiple transitions with different temperature dependence [17]. Here we assume m (>2) transitions have been selected according to the design rules proposed in our theoretical development [18] and the integrated absorbances for the selected m transitions, A_i, have been obtained from the wavelength-multiplexed (WM)-LOS absorption measurements. Two different strategies, profile fitting and temperature binning, are considered for interpreting the WM-LOS absorption data of multiple transitions for inferring nonuniform temperature distributions along the measurement path.

A. Profile Fitting

The profile-fitting strategy first requires a postulated distribution of temperature along the measurement path to constrain the temperature profile fitting. For example, in a confined combustion flow, the gas temperature often has a cold boundary layer, and the simplest representation would be a "2-T" profile with a core flow at an average temperature of T_c and a boundary layer with an average temperature of T_b and a thickness of L_b, as shown by Fig. 1a. A more complex but common representation would be a parabolic profile constrained by the center temperature of T_c and the wall temperature of T_w, as shown by Fig. 1b. Another somewhat more sophisticated model would be a uniform core flow at a temperature of T_c and a boundary layer with parabolic temperature distribution constrained by the wall temperature of T_w and the boundary layer thickness of L_b, as shown by Fig. 1c. These postulated temperature distribution profiles can be represented by a general functional form as follows:

$$T(x) = f(T_{\mathrm{char}}, L_{T\mathrm{char}}, x) \tag{9}$$

where T_{char} is the characteristic temperature such as T_c, T_w, and T_b, and $L_{T\mathrm{char}}$ is the characteristic length such as L_b. Similarly, the shape for the absorber mole-fraction distribution is also postulated using physical constraints

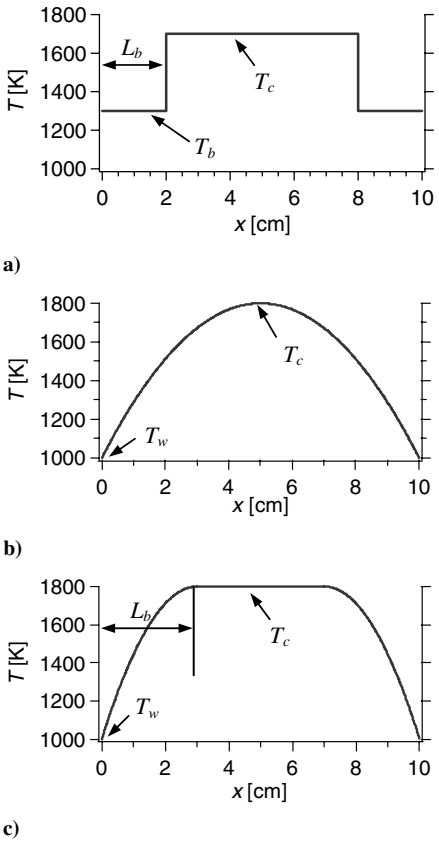

Fig. 1 Postulated temperature distribution profiles for confined combustion gases with cold walls.

$$X_{\text{abs}}(x) = g(X_{\text{char}}, L_{X\text{char}}, x) \tag{10}$$

where X_{char} is the characteristic mole fraction and $L_{X\text{char}}$ the corresponding length.

Based on the presumed temperature and mole-fraction profiles, the integrated absorbance of any transition can be calculated by substituting Eqs. (9) and (10). For the selected m transitions, a nonlinear equation set can be established:

$$\begin{cases} A_1 = P\int_0^L g(X_{\text{char}}, L_{X\text{char}}, x) S_1[f(T_{\text{char}}, L_{T\text{char}}, x)]\,\mathrm{d}x \\ A_2 = P\int_0^L g(X_{\text{char}}, L_{X\text{char}}, x) S_2[f(T_{\text{char}}, L_{T\text{char}}, x)]\,\mathrm{d}x \\ \vdots \\ A_m = P\int_0^L g(X_{\text{char}}, L_{X\text{char}}, x) S_m[f(T_{\text{char}}, L_{T\text{char}}, x)]\,\mathrm{d}x \end{cases} \tag{11}$$

Once the number of equations, i.e., the number of measured absorption transitions m, is larger than the number of unknowns, Eqs. (11) can be solved by nonlinear least-square fitting

$$\min_{T_{\text{char}}, L_{T\text{char}}, X_{\text{char}}, L_{X\text{char}}} \sum_{i=1}^{m} \left(P\int_0^L g(X_{\text{char}}, L_{X\text{char}}, x) \times S_i[f(T_{\text{char}}, L_{T\text{char}}, x)]\,\mathrm{d}x - A_i \right)^2 \tag{12}$$

to obtain the set of T_{char}, $L_{T\text{char}}$, X_{char}, and $L_{X\text{char}}$ that best describe the postulated temperature and mole-fraction profiles.

Expression (12) presents the most general mathematical model for the profile-fitting strategy. It can be simplified by using more physical constraints. For example, if the temperature nonuniformity in a combustion flow results mainly from the nonuniform local equivalence ratio, the mole-fraction distribution of the absorber, e.g., water vapor, can be assumed to be similar to the temperature distribution, i.e.,

$$g(X_{\text{char}}, L_{X\text{char}}, x) = cf(T_{\text{char}}, L_{T\text{char}}, x) \tag{13}$$

where c is a constant to be inferred from the fitting along with T_{char} and $L_{T\text{char}}$. When such relationship is used in the profile fitting, the number of unknowns will be greatly reduced. As another example, the mole fraction can be assumed to be constant along the measurement path in cases where the temperature nonuniformity is much more significant than that of the mole fraction. Finally, measurements by other sensors, CFD calculations, past knowledge on the target flowfield or a similar system, etc., can be used to constrain some of the variables and reduce the number of unknowns in the postulated temperature profile. For example, thermocouples can be used to measure the gas temperature near the wall, T_w, so that this quantity is known.

The profile-fitting strategy obviously requires using physical understanding of the flowfields to constrain the temperature and mole-fraction distributions along the measurement path. Simulation studies [18] have demonstrated that the measurement results will be greatly improved by using as many physical constraints as possible to reduce the number of unknowns in the postulated temperature profile.

B. Temperature Binning

If a priori knowledge of the flowfields is not readily accessible, the temperature-binning method can be used to extract the characteristic information on the LOS nonuniformities. The temperature-binning method is also useful for cases where the temperature distribution of the flowfields cannot be represented by a simple profile or cases where obtaining an exact temperature distribution profile is just not necessary for the application. The temperature-binning method is derived from a discretization of Eq. (5):

$$\tilde{A} = \frac{A}{P} = \sum_{j=1}^{n} [S(T_j) X_{\text{abs},j} L_j] \tag{14}$$

which implies decomposing the entire measurement path with nonuniform properties into n sections, each with a nearly uniform temperature of T_j, absorber mole fraction of $X_{\text{abs},j}$, and path length of L_j. For the selected m absorption transitions, the following linear equation set can be established:

$$\begin{bmatrix} S_1(T_1) & S_1(T_2) & \cdots & S_1(T_n) \\ S_2(T_1) & S_2(T_2) & \cdots & S_2(T_n) \\ \vdots & \vdots & \vdots & \vdots \\ S_m(T_1) & S_m(T_2) & \cdots & S_m(T_n) \end{bmatrix} \cdot \begin{bmatrix} (X_{\text{abs}}L)_1 \\ (X_{\text{abs}}L)_2 \\ \vdots \\ (X_{\text{abs}}L)_n \end{bmatrix} = \begin{bmatrix} \tilde{A}_1 \\ \tilde{A}_2 \\ \vdots \\ \tilde{A}_m \end{bmatrix} \tag{15}$$

where the n temperature bins are prescribed based on a rough estimation of the possible temperature range along the measurement path. Once the number of absorption transitions is larger than the number of temperature bins, i.e., $m > n$, Eqs. (15) can be solved by constrained linear least-square fitting

$$\min_{(X_{\text{abs}}L)_j} \sum_{i=1}^{m} \left(\sum_{j=1}^{n} [S_i(T_j)(X_{\text{abs}}L)_j] - \tilde{A}_i \right)^2 \quad \text{such that } (X_{\text{abs}}L)_j \geq 0 \quad (j = 1, \cdots n) \tag{16}$$

The solution for $(X_{\text{abs}}L)_j$, called column density [17], is actually the probability density function (PDF) of the absorbing species.

More physically meaningful results can be inferred from the PDF solution if other physical constraints are available. For example, if the mole fraction of the absorbing species can be assumed to be constant, the fraction of path length f_j for each temperature bin can be calculated from the column density because

$$f_j = \frac{(X_{\text{abs}}L)_j}{\sum_{j=1}^{n}[(X_{\text{abs}}L)_j]} = \frac{L_j}{L} \tag{17}$$

Figure 2 shows such a case where the combustion gas temperature along the measurement path has a parabolic distribution as plotted in Fig. 2a and the mole fraction of absorber can be assumed to be constant. Ten temperature bins within a typical combustion temperature of 1000–2000 K have been prescribed. Figure 2b shows the exact PDF solution, which reveals that no temperature is higher than 1800 K along the measurement path because the two highest-temperature bins are empty, and ~35% of the entire path is at the temperature of 1700–1800 K, whereas only 6% is at 1000–1100 K, etc. This example serves to illustrate that nonintrusive and rapid

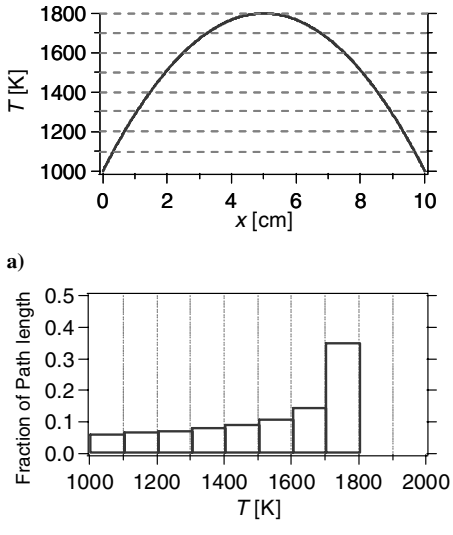

Fig. 2 a) Parabolic temperature distribution and b) the temperature-binning result for this distribution.

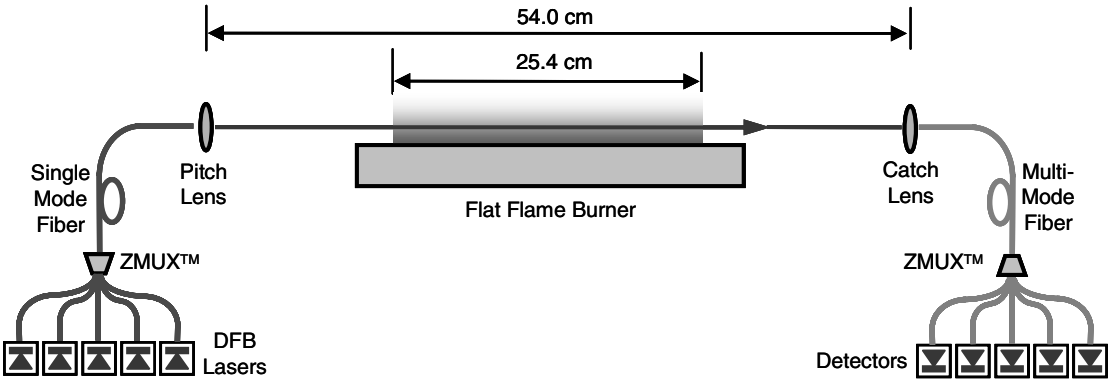

Fig. 3 Schematic of the experimental setup for a five-laser multiplexed absorption sensor.

measurements of this type may be useful in characterizing channel flows, e.g., in connection with process control.

Simulation studies [18] have shown that increasing the number of bins n (for fixed number of transitions m) will deteriorate the measurement accuracy. Thus a moderate number of bins, e.g., five, should be initially used and more bins justified only if more transitions can be measured. In spite of the limited number of bins and the lack of information on the spatial arrangement of the bins along the path, the PDF solution is sufficient for many monitoring and control applications where the goal focuses on minimizing or maximizing the nonuniformities, e.g., pattern factor sensing and control [16], or on monitoring the fluctuations in the PDF solution in, e.g., turbulent studies [18].

III. Demonstration Experiments

The two strategies to interpret LOS absorption measurements in flows with a nonuniform temperature distribution are demonstrated by laboratory measurements of a two-zone temperature distribution with a wavelength-multiplexing (WM) scheme. H_2O vapor is selected as the absorbing species because it is naturally present in the atmosphere, it is a major product of hydrocarbon combustion, and it has strong rovibrational overtone transitions in the near-infrared that overlap with readily available telecommunication diode lasers.

A. Two-Zone Temperature/Mole-Fraction Distribution

A two-zone temperature LOS experiment is conducted to illustrate the measurement and data analysis concepts. The schematic of the experiment is shown in Fig. 3. The free space laser beam has a total path length of 54 cm set by the spacing between the pitch lens and the catch lens. A 25.4-cm-long flat-flame burner is located at the center of the measurement path to create a uniform hot section. Therefore, the entire LOS measurement path can be roughly divided into two zones, one in the cold room air and the other in the hot-flame gases. This experimental arrangement is illustrative of combustion flows with confined flames that do not completely fill the flame chamber or duct. Figure 4 shows the thermocouple measurements of this steady, nonuniform temperature distribution along the laser beam path. The water mole fraction is ~10% in the high-temperature zone and ~1.75% in the room-temperature zone as listed in Table 1.

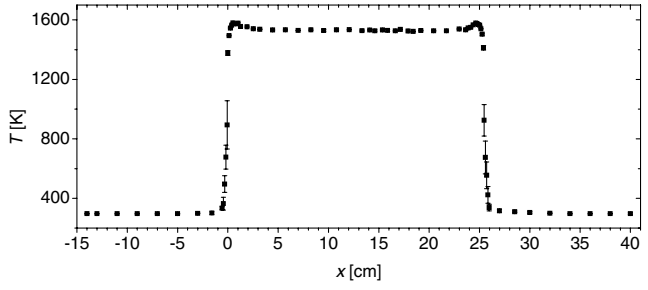

Fig. 4 Thermocouple measurements of the nonuniform temperature distribution along the laser beam path.

The flat-flame burner is fueled by premixed ethylene and dry air. Because of its special design [21], a stable laminar flame can be obtained over the equivalence ratio range of 0.6–1.4. For the current demonstration experiments, the ethylene and air flow rates are measured to be 1.8 standard liters per minute (slm) and 34.0 slm, respectively, by calibrated rotameters. The equivalence ratio is thus 0.76, which leads to an equilibrium water vapor mole fraction of 10.0% with an uncertainty of ~3% due to the measurement uncertainty of the fuel-/airflow rates.

The flame temperature is measured at the height of the laser beam (~5 mm above the burner surface) by a type S thermocouple with a bead size of 2 mil (~51 μm). The radiation corrections for the thermocouple readings are ~55 K [22]. As shown by Fig. 4, the core part of the flame (1–24 cm) has a uniform temperature distribution. The average is ~1534 K, with an uncertainty of ~3% estimated from the scatter of the thermocouple readings and the uncertainty in the radiation correction. This measured flame temperature is lower than the adiabatic flame temperature at the measured equivalence ratio mainly due to the radiation loss to the surroundings and the heat conduction to the water-cooled burner surface. At both edges of the flame, there is a very slight temperature rise and then a sharp drop to the room temperature, thus creating well-defined high- and low-temperature zones along the LOS measurement path.

The thermocouple measurement of the room temperature is ~298 K, which agrees with the readings of a mercury thermometer. The room air humidity is measured by a calibrated hygrometer to be ~56%, which indicates a water mole fraction of ~1.75%. The temperature, water mole fraction, and path length of the two zones are summarized in Table 1.

B. Wavelength-Multiplexed Diode-Laser Absorption Measurements

The layout of the WM scheme is also shown in Fig. 3. The fiber-coupled outputs from five distributed-feedback (DFB) InGaAsP lasers (NEL NLK1B5E1AA, 10–30 mW) are combined together and coupled into one single-mode fiber by a multiplexer (Zolo Technologies, ZMUX™, ZD1549-A). The multiplexed laser beam is then collimated by the pitch lens (Thorlabs F220FC-C) and propagates across the two-zone measurement path. Another lens (Thorlabs F220FC-C) installed in a five-axis mount is used to catch the free space laser beam and focus it into a multimode fiber, which leads to a grating-based demultiplexer (Zolo Technologies, ZMUX™, ZD1550-A). The wavelength-multiplexed beam is then diffracted into the constituent five wavelengths, collected on fiber for each channel and delivered to five InGaAs detectors (Thorlabs PDA400).

Table 1 Expected properties of the two-zone temperature distribution along the line-of-sight measurement path

	Zone 1	Zone 2
T, K	298 (±1)	1534 (±50)
X_{H2O}, %	1.75 (±0.05)	10.0 (±0.3)
L, cm	28.6 (±0.2)	25.4 (±0.2)

Table 2 Spectroscopic parameters of the seven water vapor transitions used in the demonstration experiments

Line index	ν_0, cm^{-1}	$S(T_0)$, cm^{-2} atm^{-1}	E'', cm^{-1}
1	7154.35	3.670E − 04	1789.04
2	7164.90	3.550E − 03	1394.81
3	7185.60	1.960E − 02	1045.06
4	7417.82	1.070E − 02	1079.08
5	7444.36	1.100E − 03	1786.00
6	7164.07	2.021E − 02	300.36
7	7419.17	2.222E − 02	842.36

The five DFB lasers emit near 1343, 1345, 1392, 1395, and 1398 nm. These wavelengths are chosen to be compatible with five channels of the two Zolo ZMUX^{TM} products. The fiber-coupled, echelle grating-based ZMUX^{TM} multi/demultiplexers are chosen over free space, conventionally ruled gratings because these compact devices allow dense wavelength multiplexing and demultiplexing (up to 44 wavelengths) with high efficiency, preset alignment, and well-controlled polarization-dependent loss and thermal drift.

The DFB lasers can be scanned across 2–3 cm^{-1} by injection current variation, enabling access to the seven strong water vapor transitions listed in Table 2 and indicated in Fig. 5. These seven transitions are used for this experiment to illustrate the proposed sensor concepts and demonstrate the feasibility, though they are not the optimum choice for the current temperature range. For future applications, improved transitions can be selected according to the design rules proposed separately [18], and the ZMUX^{TM} multi/demultiplexer can be customized accordingly. Besides the WM scheme, the selected optimal transitions could also be accessed by wide-wavelength-scanning laser sources, such as vertical cavity surface emitting lasers (VCSEL) [17] and external cavity diode lasers (ECDL) [18,23].

Each DFB laser (14-pin butterfly package) is installed in a ILX Lightwave mount (LDM-4984) with its current and temperature controlled by one channel of an ILX Lightwave diode-laser controller (LDC-3900). All five lasers are simultaneously scanned at 1 kHz with a linear current ramp. The transmitted laser signals obtained by the five detectors are simultaneously recorded at a 5 MHz sampling rate by two synchronized NI DAQ cards using a Labview scope program. The wavelength of each laser scan has been precalibrated using a solid etalon with a free spectral range (FSR) of 2.00 GHz [19].

C. Data Reduction

The recorded raw-data scans from each of the five channels are corrected for detector DC offsets and background emission, although most of the emission from the flame has been rejected by the ZMUX^{TM} demultiplexer, which acts as a band-pass filter with a narrow bandwidth of ∼1 nm for each channel. The corrected raw data for each channel are then averaged for every 10 sequential scans to reduce stochastic noise. The resulting time response of this demonstration measurement is 10 ms, owing to the 10-sweep average of the 1 kHz wavelength scans. (Note that this time response is not a maximum for the technique, as we have routinely made scanned-wavelength direct absorption measurements at 10 kHz [24] and have performed limited demonstration measurements at scan rates of 50 kHz [25].) From each averaged laser scan (i.e., the transmitted signal I_t), the unattenuated laser intensity (i.e., the baseline I_0) is determined by fitting the part of the I_t trace without absorption with a polynomial [19]. The absorption spectrum is then calculated using Eq. (4). Figure 5 shows an example of the reduced absorption spectra for each of the five channels.

The integrated absorbances A_i for the seven lines are then calculated from the measured absorption spectra. The data reduction is more complicated than that for uniform cases [19] because the line shape measured along a nonuniform temperature distribution can no longer be modeled by a single Voigt function. Instead of doing least-square fitting using multiple Voigt functions, which would be computationally expensive, a hybrid Voigt fit scheme similar to that proposed previously [17] is employed in this work, as illustrated in Fig. 6. First, the side wings of the target line shape, excluding the ∼0.1 cm^{-1} center portion marked by the vertical dashed line, are Voigt fit to minimize the residual shown on the top panel of Fig. 6. The area obtained is denoted as A_{Voigt}, and has excluded contributions from neighboring features. Besides the collision width and line-center frequency, the width of the center portion and the Doppler width of the Voigt function are also free parameters of the

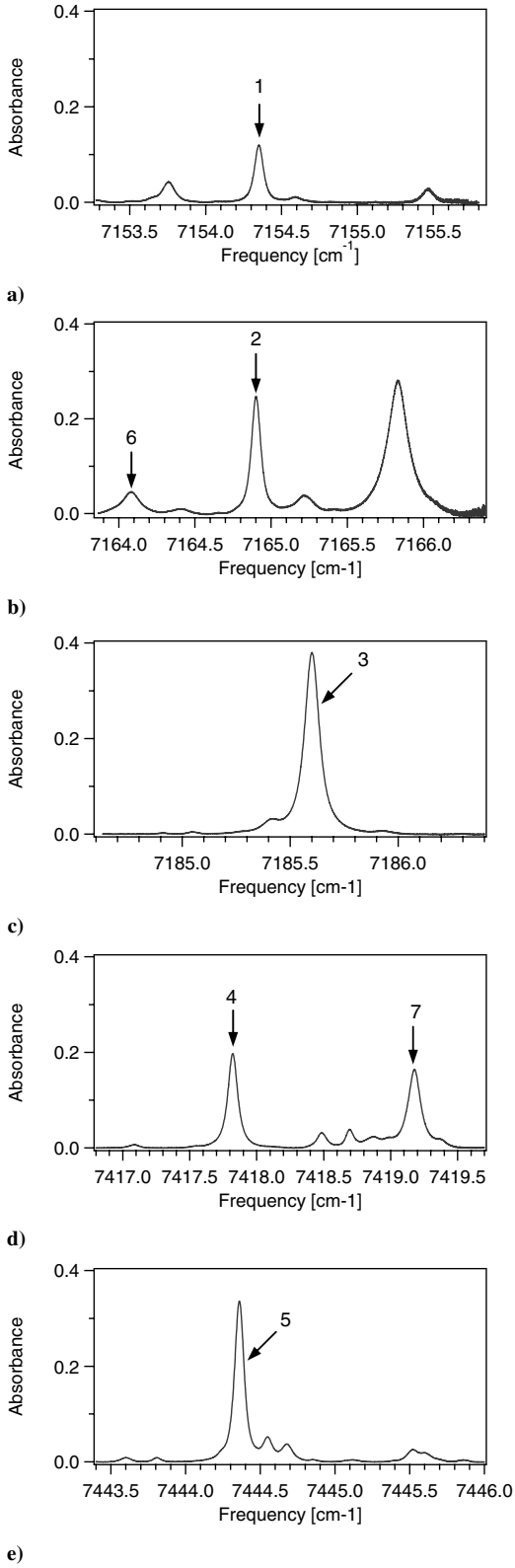

Fig. 5 Absorption spectra for five lasers using setup from Fig. 3 and conditions from Table 1.

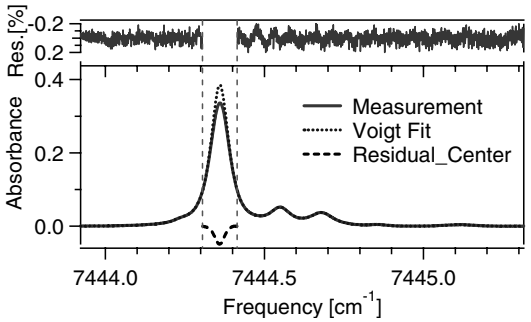

Fig. 6 Illustration of hybrid Voigt fit using measured line shape of transition 5.

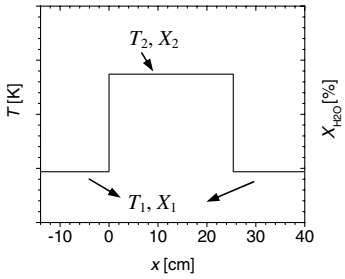

Fig. 7 Two-zone property distribution postulated for profile-fitting calculation.

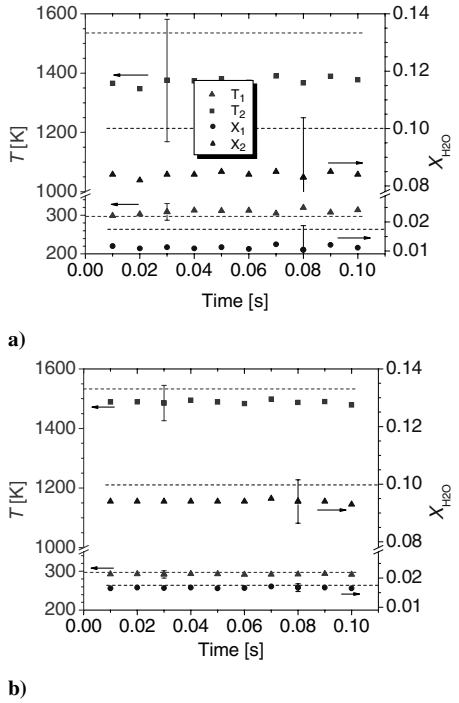

Fig. 8 Case 1, profile fitting: T_1, T_2, X_1, X_2 fit a) lines 1–5; b) lines 1–7.

least-square fit. The difference between the Voigt fit and the measured line shape, as shown by the dash curve plotted in Fig. 6, is numerically integrated to obtain A_{residual}. The total integrated absorbance for the target line is thus the sum of A_{Voigt} and A_{residual}.

Once the integrated absorbances for the seven lines are obtained, either the profile-fitting strategy or the temperature-binning strategy can be applied to characterize the nonuniform temperature distribution using the models introduced in Sec. II. The spectroscopic parameters of the seven transitions used in the calculations are listed in Table 2, in which the values for lines 1–5 are taken from [26] and the others from HITRAN 2004 [27].

IV. Results and Discussion

If we assume that both the temperature and water mole fraction along the LOS measurement path are uniform, this "uniform" temperature can be inferred from the measured absorbances of any line pair as per Eq. (8). Here line pair 1 and 2 yields 1199 K, whereas line pair 1 and 3 produces 1122 K. This discrepancy suggests nonnegligible nonuniformities [16], thus illustrating the value of the new strategy to use multiple absorption measurements to characterize the actual temperature distribution.

A. Profile-Fitting Results

In the profile-fitting calculation, the shape of the nonuniform property distribution must be postulated in advance. The layout of the experimental setup (hot-flame temperature in the middle with cold room temperatures on both sides) enables us to postulate a two-zone profile as shown in Fig. 7 to model the temperature and mole-fraction distribution along the LOS measurement path. The unknowns (free parameters) to be solved from the multiple absorption measurements are the temperature and mole fraction for each zone, i.e., T_1, T_2, X_1, and X_2. We investigate four different interpretations of the measured absorption data, each with a different number of constraints on the postulated distributions. For each of these four cases, the influence of the number of lines on the sensor performance is investigated.

In case 1, the measured absorbances are fit as per Eq. (12) with all four unknowns T_1, T_2, X_1, and X_2 as free parameters. A time series of 10 individual results are shown in Fig. 8 and the average values are listed in Table 3. The results using lines 1–5 and lines 1–7 are shown in Figs. 8a and 8b, respectively. The dashed lines represent the expected values. The error bars indicate the measurement uncertainty estimated based on the uncertainties in the spectroscopic parameters, the measured integrated absorbance for each line, and the solution of the nonlinear least-square fit. The details for estimating the measurement uncertainties can be found in the simulation studies in [18]. Both the measurement accuracy, as indicated by the difference between the measured and the expected values, and the statistical precision, as indicated by the scatter of the fitting results over the 10 independent measurements, increase appreciably with the addition of data from lines 6 and 7. By using the absorbances measured on lines 1–5, the temperature and mole fraction inferred deviate significantly from the expected values, which is partly due to the narrow span of the lower-state energy E'' of these five transitions. By adding measurements from line 6 and 7 with much lower E'', the results for T_1, T_2, X_1, and X_2 quickly converge to the expected values within an accuracy of 2, 3, 3, and 6%, respectively. This result illustrates the importance of optimized selection of absorption transitions [18].

In case 2, the H_2O mole faction of the cold zone X_1 is fixed at 1.75%, which is determined using the measured humidity and an estimated temperature (300 K) of the room air. The three remaining unknowns T_1, T_2, and X_2 are then allowed to vary in the nonlinear least-square fit. A time series of 10 individual results are shown in Fig. 9 and the average values are listed in Table 3. Again the measurement accuracy increases systematically with the addition of data from lines 6 and 7. By using all seven transitions, the T_1, T_2, and X_2 can be measured within an accuracy of 1, 1, and 3%, respectively, which improves from the corresponding results for case 1. Generally speaking, the addition of physical constraint(s) improves the accuracies of the fit values [18]. The model simulations in [18] illustrate the significant tolerance of the fits for a $\pm 10\%$ range of constrained values.

In case 3, the H_2O mole fractions for the two zones X_1 and X_2 are fixed at 1.75 and 10% (the equilibrium value for the measured equivalence ratio), respectively. Because there are only two remaining unknowns, T_1 and T_2, a minimum number of three lines are required for the nonlinear least-square fit. A time series of 10 individual results are shown in Fig. 10 and the average values are listed in Table 4. These fit results reveal the same trend, namely, an increasing of the accuracy of the fit values with an increased number of lines. Even with the minimum number of lines, however,

Table 3 Average values of the profile-fitting results (and percentage deviation from the expected values) with different number of lines for cases 1 and 2

Lines	Case 1				Case 2		
	T_1, K	T_2, K	X_1, %	X_2, %	T_1, K	T_2, K	X_2, %
1–5	309 (4%)	1374 (−10%)	1.1 (−37%)	8.4 (−16%)	227 (−24%)	1264 (−18%)	7.8 (−22%)
1–7	292 (−2%)	1489 (−3%)	1.7 (−3%)	9.4 (−6%)	295 (−1%)	1524 (−1%)	9.7 (−3%)
Expected	298	1534	1.75	10.0	298	1534	10.0

satisfactory results of T_1 and T_2 can be obtained (with an accuracy of 4 and 1%, respectively) by fixing the H_2O mole-fraction values.

In case 4, the properties of the room air T_1 and X_1 are fixed in the fit, and thus only the properties of the hot-flame zone T_2 and X_2 are the free parameters. A time series of 10 individual solutions are shown in Fig. 11 and the average values are listed in Table 4. Again, the accuracy increases with the number of lines, and particularly with the inclusion of lines 6 and 7. Using all seven transitions, the T_2 and X_2 are determined within an accuracy of 1 and 2%, respectively.

This two-zone measurement arrangement is clearly applicable to cases with interference absorption by humid room air bounding a relatively uniform hot zone of interest. Only the temperature and water content of the hot target gas is typically desired, but sometimes room air is inevitably enclosed in the LOS beam path near the pitch or catch optics, because the laser sources or the measurement geometries prohibit using fibers to deliver the laser beam directly to the edge of the flowfields to be measured. Normally, in our laboratory, the open path in this boundary is purged with N_2 to remove the interference absorption by the room air [13], but the purging efficiency cannot always be guaranteed, especially if the purging system is not well designed, installed, and maintained. By using more than two transitions as was done in case 4, the flowfield properties of interest can be inferred directly from the LOS absorption data without installing complex purging systems.

Table 5 shows a comparison of the profile fitting results for all four cases when data from all seven transitions are used. It confirms that the fitting results improve significantly when the number of unknowns (free parameters) in the postulated distribution profiles can be reduced by using physical constraints.

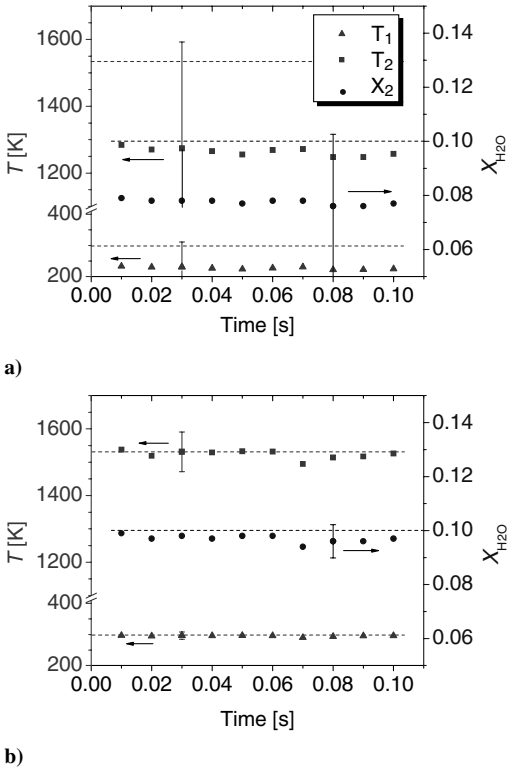

Fig. 9 Case 2, profile fitting: X_1 fixed, T_1, T_2, X_2 fit a) lines 1–5; b) lines 1–7.

B. Temperature-Binning Results

Alternatively, we can interpret the absorption data using the temperature-binning strategy. An estimation of the possible temperature range along the LOS measurement path allows the prescription of five temperature bins as shown in Fig. 12. All seven transitions are used in the analysis. The resultant column densities $(X_{H2O}L)_j$, as represented by the solid bars, are very close to the expected PDF solutions, as indicated by the dash-dot lines. Only the two side bins have nonzero solutions. They suggest that the LOS measurement path can be approximately modeled as two zones, one at ∼300 K and the other at ∼1500 K, which are very close to the conditions of the experiment. The population of water vapor in the highest-temperature bin is much larger than that in the lowest-temperature bin, which implies that the "2-T" distribution might

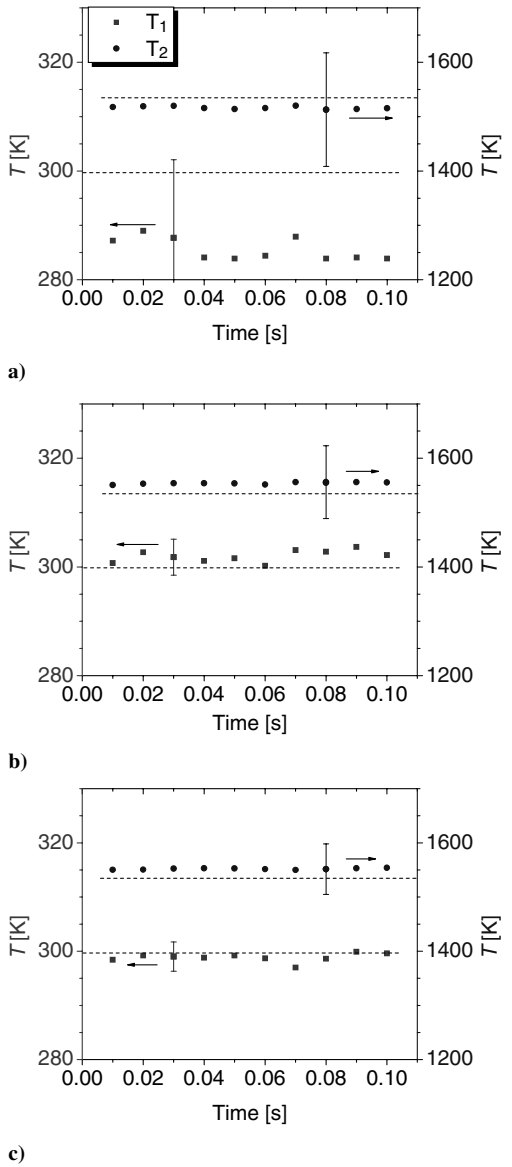

Fig. 10 Case 3, profile fitting: X_1, X_2 fixed, T_1, T_2 fit a) lines 1–3; b) lines 1–5; c) lines 1–7.

Table 4 Average values of the profile-fitting results (and percentage deviation from the expected values) with different number of lines for cases 3 and 4

Lines	Case 3		Case 4	
	T_1, K	T_2, K	T_2, K	X_2, %
1–3	286 (−4%)	1516 (−1%)	1487 (−3%)	9.4 (−6%)
1–5	302 (1%)	1554 (1%)	1520 (−1%)	9.6 (−4%)
1–7	299 (0%)	1552 (1%)	1537 (0%)	9.8 (−2%)
Expected	298	1534	1534	10.0

result from a cold spot somewhere along an otherwise uniform high-temperature region or a cold boundary layer on both sides of a uniform hot core temperature. Note that, up to this point, no a priori knowledge of the flowfields, except for an estimate of the possible temperature range, has been applied to extract the characteristic information on the LOS nonuniformities discussed earlier in this paper.

V. Summary

This paper reports an initial laboratory demonstration of two strategies for measurements of nonuniform temperature distributions using line-of-sight absorption spectroscopy. Based on the measurements of multiple absorption transitions with different temperature dependences, the profile-fitting strategy fits a postulated temperature distribution profile, whereas the temperature-binning strategy determines the temperature probability density function along the LOS using prescribed temperature bins. Both strategies can be mathematically modeled as least-square fitting problems. In the nonoptimized demonstration experiment, a two-zone temperature/mole-fraction distribution created in laboratory is measured with a wavelength-multiplexing scheme where five DFB diode lasers are multiplexed to probe seven absorption transitions of water vapor with a 1 kHz measurement rate. Note that measurement rates up to 50 kHz are possible with modern telecommunications-grade diode lasers [25]. The absorption data are analyzed by both strategies to illustrate the sensor concepts and investigate the sensor performance. The experimental results presented in this paper demonstrate that a nonuniform temperature distribution can be characterized with either strategy by measuring the LOS absorption for a limited number of transitions with different temperature dependences. The measurement accuracies will increase with the number of transitions, and also with the use of optimally chosen transitions. Use of known physical constraints also provides important value in properly interpreting measurement results and improving the sensor performance.

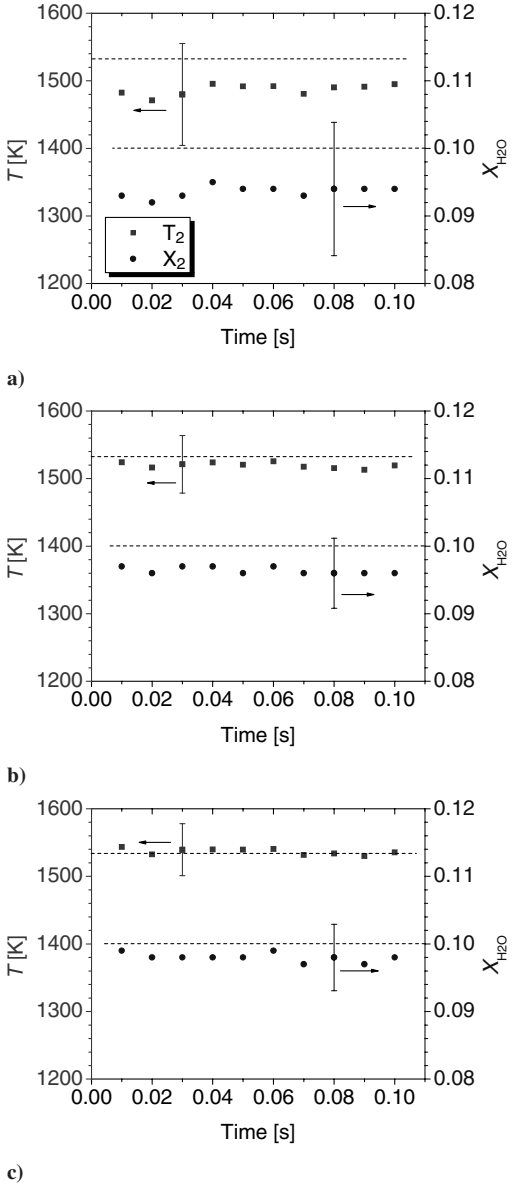

Fig. 11 Case 4, profile fitting: T_1, X_1 fixed, T_2, X_2 fit a) lines 1–3; b) lines 1–5; c) lines 1–7.

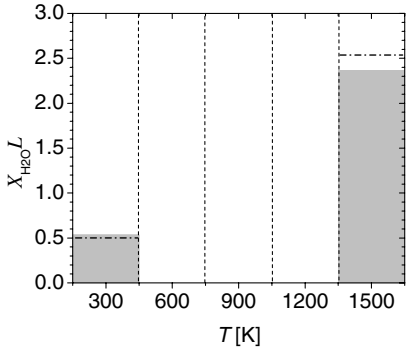

Fig. 12 Illustration of temperature-binning results solved using all seven transitions with five bins.

Table 5 Comparison of the profile-fitting results (and percentage deviation from the expected values) for all four cases with all seven lines

Case	T_1, K	T_2, K	X_1, %	X_2, %
1	292 (−2%)	1489 (−3%)	1.7 (−3%)	9.4 (−6%)
2	295 (−1%)	1524 (−1%)	——	9.7 (−3%)
3	299 (0%)	1552 (1%)	——	——
4	——	1537 (0%)	——	9.8 (−2%)
Expected	298	1534	1.75	10.0

Acknowledgments

We gratefully acknowledge support from the Air Force Office of Scientific Research (AFOSR) with Julian Tishkoff as technical monitor and via an Air Force STTR with Zolo Technologies, and from Stanford through the Global Climate and Energy Project. We thank Hejie Li for laboratory assistance with the flat-flame burner.

References

[1] Allen, M. G., "Diode Laser Absorption Sensors for Gas-Dynamic and Combustion Flows," *Measurement Science and Technology*, Vol. 9, No. 4, 1998, pp. 545–562.

[2] Baer, D. S., Newfield, M. E., Gopaul, N., and Hanson, R. K., "Multiplexed Diode-Laser Sensor System for Simultaneous H_2O, O_2, and Temperature Measurements," *Optics Letters*, Vol. 19, No. 22, 1994, pp. 1900–1902.

[3] Mihalcea, R. M., Baer, D. S., and Hanson, R. K., "Advanced Diode Laser Absorption Sensor for In-Situ Combustion Measurements of CO_2, H_2O, and Gas Temperature," *Proceedings of the Combustion Institute*, Vol. 27, 1998, p. 95.

[4] Sanders, S. T., Baldwin, J. A., Jenkins, T. P., Baer, D. S., and Hanson, R. K., "Diode Laser Sensor for Monitoring Multiple Combustion Parameters in Pulse Detonation Engines," *Proceedings of the Combustion Institute*, Vol. 28, 2000, pp. 587–594.

[5] Ebert, V., Fernholz, T., Giesemann, C., Pitz, H., Teichert, H., Wolfrum, J., and Jaritz, H., "Simultaneous Diode-Laser-Based In Situ Detection of Multiple Species and Temperature in a Gas-Fired Power Plant," *Proceedings of the Combustion Institute*, Vol. 28, 2000, pp. 423–430.

[6] Teichert, H., Fernholz, T., and Ebert, V., "Simultaneous In Situ Measurement of CO, H_2O, and Gas Temperatures in a Full-Sized Coal-Fired Power Plant by Near-Infrared Diode Lasers," *Applied Optics*, Vol. 42, No. 12, 2003, pp. 2043–2051.

[7] Ravichandran, M., and Gouldin, F. C., "Determination of Temperature and Concentration Profiles Using (a Limited Number of) Absorption Measurements," *Combustion Science and Technology*, Vol. 45, Nos. 1–2, 1986, pp. 47–64.

[8] Kauranen, P., Hertz, H. M., and Svanberg, S., "Tomographic Imaging of Fluid Flows by the Use of Two-Tone Frequency-Modulation Spectroscopy," *Optics Letters*, Vol. 19, No. 18, 1994, pp. 1489–1491.

[9] Zhang, F. Y., Fujiwara, T., and Komurasaki, K., "Diode-Laser Tomography for Arcjet Plume Reconstruction," *Applied Optics*, Vol. 40, No. 6, 2001, pp. 957–964.

[10] Villarreal, R., and Varghese, P. L., "Frequency Resolved Absorption Tomography with Tunable Diode Lasers," *Applied Optics*, Vol. 44, No. 31, 2005, pp. 6786–6795.

[11] Schoenung, S. M., and Hanson, R. K., "CO and Temperature Measurements in a Flat Flame by Laser Absorption Spectroscopy and Probe Techniques," *Combustion Science and Technology*, Vol. 24, Nos. 5–6, 1981, pp. 227–137.

[12] Ouyang, X., and Varghese, P. L., "Line-of-Sight Absorption Measurements of High Temperature Gases with Thermal and Concentration Boundary Layers," *Applied Optics*, Vol. 28, No. 18, 1989, pp. 3979–3984.

[13] Zhou, X., Liu, X., Jeffries, J. B., and Hanson, R. K., "Development of a Sensor for Temperature and Water Concentration in Combustion Gases Using a Single Tunable Diode Laser," *Measurement Science and Technology*, Vol. 14, No. 8, 2003, pp. 1459–1468.

[14] Wang, J., Maiorov, M., Jeffries, J. B., Garbuzov, D. Z., Connolly, J. C., and Hanson, R. K., "A Potential Remote Sensor of CO in Vehicle Exhausts Using 2.3 Micron Diode Lasers," *Measurement Science and Technology*, Vol. 11, No. 11, 2000, pp. 1576–1584.

[15] Seitzman, J. M., and Scully, B. T., "Broadband Infrared Absorption Sensor for High-Pressure Combustor Control," *Journal of Propulsion and Power*, Vol. 16, No. 6, 2000, pp. 994–1001.

[16] Palaghita, T., and Seitzman, J. M., "Pattern Factor Sensing and Control Based on Diode Laser Absorption," AIAA Paper 2005-3578, July 2005.

[17] Sanders, S. T., Wang, J., Jeffries, J. B., and Hanson, R. K., "Diode-Laser Absorption Sensor for Line-of-Sight Gas Temperature Distributions," *Applied Optics*, Vol. 40, No. 24, 2001, pp. 4404–4415.

[18] Liu, X., "Line-of-Sight Absorption of H_2O Vapor: Gas Temperature Sensing in Uniform and Non-Uniform Flows," Ph.D. Dissertation, Mechanical Engineering Dept., Stanford Univ., Stanford, CA, 2006, http://thermosciences.stanford.edu/pdf/TSD-168.pdf [cited 20 Nov. 2006].

[19] Liu, X., Jeffries, J. B., Hanson, R. K., Hinckley, K. M., and Woodmansee, M. A., "Development of a Tunable Diode Laser Sensor for Measurements of Gas Turbine Exhaust Temperature," *Applied Physics B, Lasers and Optics*, Vol. 82, No. 3, 2006, pp. 469–478.

[20] Gamache, R. R., Kennedy, S., Hawkins, R., and Rothman, L. S., "Total Internal Partition Sums for Molecules in the Terrestrial Atmosphere," *Journal of Molecular Structure*, Vol. 517–518, 2000, pp. 407–425.

[21] Mihalcea, R. M., "CO and CO_2 Measurements in Combustion Environments Using External Cavity Diode Lasers," Ph.D. Dissertation, Mechanical Engineering Dept., Stanford Univ., Stanford, CA, 1999.

[22] Shaddix, C. R., "Correcting Thermocouple Measurements for Radiation Loss: A Critical Review," American Society of Mechanical Engineers Paper HTD99-282, Aug. 1999.

[23] Liu, X., Zhou, X., Jeffries, J. B., and Hanson, R. K., "Experimental Study of H_2O Spectroscopic Parameters in the Near-IR," AIAA Paper 2005-0829, Jan. 2005.

[24] Rieker, G. B., Li, H., Liu, X., Liu, J. T. C., Jeffries, J. B., Hanson, R. K., Allen, M. G., Wehe, S. D., Mulhall, P. A., Kindle, H. S., Kakuho, A., Sholes, K. R., Matsuura, T., and Takatani, S., "Rapid Measurements of Temperature and H_2O Concentrations in IC Engines with a Spark Plug-Mounted Diode Laser Sensor," *Proceedings of the Combustion Institute* (to be published).

[25] Houle, A. J., Nakakita, K., Heltsley, W. N., Jeffries, J. B., and Hanson, R. K., "Diode Laser Absorption Measurements of Supersonic Flow in an Experimental Tube," AIAA Paper 2006-4444, July 2006.

[26] Liu, J. T. C., Rieker, G. B., Jeffries, J. B., and Hanson, R. K., "Near-Infrared Diode Laser Absorption Diagnostic for Temperature and Water Vapor in a Scramjet Combustor," *Applied Optics*, Vol. 44, No. 1, 2005, pp. 6701–6711.

[27] Rothman, L. S., Jacquemart, D., Barbe, A., Benner, D. C., Birk, M., Brown, L. R., Carleer, M. R., Chackerian, C., Jr., Chance, K., Coudert, L. H., Dana, V., Devi, V. M., Flaud, J.-M., Gamache, R. R., Goldman, A., Hartmann, J.-M., Jucks, K. W., Maki, A. G., Mandin, J.-Y, Massie, S. T., Orphal, J., Perrin, A., Rinsland, C. P., Smith, M. A. H., Tennyson, J., Tolchenov, R. N., Toth, R. A., Vander Auwera, J., Varanasi, P., and Wagner, G., "The HITRAN 2004 Molecular Spectroscopic Database," *Journal of Quantitative Spectroscopy and Radiative Transfer*, Vol. 96, No. 2, 2005, pp. 139–204.

R. Lucht
Associate Editor